without undue concern as long as the excursion is reasonable. Other existing data should be compared with the correlations to help determine the extent of applicability. If mixed compression is involved, the throat Mach number and area should be replaced by appropriate inlet-plane values. In any case, the correlations should permit an increased level of confidence in predicting cowl suction for this and other two-dimensional inlets designed for both supersonic and subsonic operation.

Conclusions

1) The linear bow-shock-position theory in conjunction with the plane supersonic inlet-flowfield Mach number has been shown to overpredict the bow-shock position of a two-dimensional inlet with swept side plates. 2) An empirical modification of the linear theory has been made that predicts the bow-shock position of the test model with reasonable consistency. 3) Possible three-dimensional flow effects in the external supersonic flowfield of a two-dimensional inlet must be considered when selecting a reference Mach number for computing bow-shock position. 4) The error in predicting the additive drag of a supersonic inlet due to inaccurate bow-shock location at low supersonic Mach numbers can be significant. 5) Cowl suction correlations not previously available have been produced from experimental data that should be useful to the inlet designer and should increase the confidence level in making this estimate for two-dimensional inlets.

References

[1] Moeckel, W. E., "Approximate Method for Predicting Form and Location of Detached Shock Waves Ahead of Plane or Axially Symmetric Bodies," TN 1921, July 1949, NACA.

[2] Petersen, M. W. and Tamplin, G. C., "Experimental Review of Transonic Spillage Drag of Rectangular Inlets," Rept. NA-66-10, North American Aviation Inc.; U.S. Air Force Rept APL-TR-66-30, May 1966.

[3] Ames Research Staff, "Equations, Tables, and Charts for Compressible Flow," Rept. 1135, 1953, NACA.

MAY-JUNE 1968 J. AIRCRAFT VOL. 5, NO. 3

Structure of Trailing Vortices

BARNES W. MCCORMICK*
The Pennsylvania State University, University Park, Pa.

JAMES L. TANGLER†
U.S. Army, San Francisco, Calif.

AND

HAROLD E. SHERRIEB‡
LTV Aerospace Corporation, Dallas, Texas

A study of aircraft trailing vortex systems, involving actual flight testing as well as model testing and analytical considerations, has resulted in a method for predicting the vortex geometry and velocity field downstream of an aircraft. It is found that the vortex decay can be described by geometric similarity considerations and not by any modification of the Navier-Stokes equations. This conclusion is based on detailed velocity measurements made through the vortex immediately behind a test aircraft up to distances of approximately 1000 chord lengths downstream of the aircraft. This report includes a presentation of the data on which the conclusions are based, as well as a description of test equipment and procedures.

Nomenclature

a = core radius [radius where $v(r)$ is a maximum]
a_0 = initial value of the core radius immediately behind the wing
b = wing span
c_0 = midspan chord
$\bar{c}$ = mean chord = S/b
E = kinetic energy of vortex system/unit length
n = exponent in vorticity distribution, Eq. (23)
r = radial distance from center of vortex; also coordinate coincident with vortex radius but arbitrary origin (Fig. 9)
r_∞ = pseudo-radius where $\Gamma(r) = \Gamma_\infty$
S = wing planform area
t = time
t' = dimensionless time, Eq. (8)
$v(r)$ = tangential velocity at radius r
v = maximum value of $v(r) = v(a)$
v_0 = value of v immediately behind the wing
V = aircraft velocity
w = half-radius = r at which $\zeta = \zeta_0/2$
w_0 = value of w for $t = 0$
Y = distance along line through vortex center
Z = distance downstream of wing trailing edge
$\gamma(2/n)$ = gamma function with argument $(2/n)$
Γ = circulation at any radius
Γ_∞ = total circulation (as $r \to \infty$)
ν = kinematic viscosity
ν_e = effective kinematic viscosity
ω = angular velocity of fluid
ω_v = angular velocity of vanes
ζ = vorticity at any radius
ζ_0 = center value of $\zeta(r = 0)$
ζ_{0I} = value of ζ_0 immediately behind wing

Received October 19, 1967; revision received January 31, 1968. This project was supported by the U.S. Army Research Office (Durham) under Contract DA-31-124-ARO (D)-149. Our appreciation is extended to D. M. May, A. H. Logan, T. L. Grow, and H. Smith for their contributions.

* Professor of Aerospace Engineering. Associate Fellow AIAA.
† Captain.
‡ Aerodynamics Design Engineer. Associate Member AIAA.

Introduction

THE vortex system shed from an aircraft wing, or from a helicopter rotor, rolls up rapidly downstream of the aircraft to form two, oppositely rotating vortices. These vortices may persist for some time after their generation and can pose a hazard to other aircraft that penetrate them. The problem of vortex interaction will be an increasingly important one as air-traffic density increases. Also the advent of the so-called "jumbo-jets" will heighten the intensity of the problem.

The problem that this paper treats is that of predicting the timewise variation of the velocity field associated with a trailing vortex generated by an aircraft of given weight, geometry, and operating conditions. The paper summarizes the results of a three-year study involving model and in-flight testing together with some limited analytical studies.

Analytical Considerations

The Navier-Stokes equation for two-dimensional axisymmetric flow can be written in terms of the vorticity as

$$\partial\zeta/\zeta t = \nu\,[\partial^2\zeta/\partial r^2 + (1/r)(\partial\zeta/\partial r)] \tag{1}$$

Assume that the solution to the preceding is of the form

$$\zeta = \zeta_0(t)\,\{\exp - [r/w(t)]^2 \ln 2\} \tag{2}$$

i.e., ζ_0 and w are functions of t. w will be referred to as the "half-radius" and is the value of r for which $\zeta = \zeta_0/2$.

The vorticity, tangential velocity v, and circulation Γ are related by

$$\zeta = (1/r)[d(vr)/dr] = (1/2\pi r)(d\Gamma/dr) \tag{3}$$

Hence,

$$\Gamma(R) = \int_0^R 2\pi r\zeta dr \tag{4}$$

$$v(R) = \frac{1}{R}\int_0^R r\zeta dr \tag{5}$$

It follows then that

$$\zeta = \frac{\zeta_{0I}}{1+t'}\exp\left[-\left(\frac{r}{w_0}\right)^2\frac{\ln 2}{1+t'}\right] \tag{6}$$

$$v(r) = \frac{w_0\zeta_{0I}}{2(r/w_0)\ln 2}\left[1 - \left\{\exp - \left(\frac{r}{w_0}\right)^2\frac{\ln 2}{1+t'}\right\}\right] \tag{7}$$

$$\Gamma = \frac{\pi w_0^2\zeta_{0I}}{\ln 2}\left[1 - \exp\left\{-\left(\frac{r}{w_0}\right)^2\frac{\ln 2}{1+t'}\right\}\right] \tag{8}$$

where $t' = t[4\nu \ln 2/w_0^2]$. The preceding equations represent a solution of the Navier-Stokes equations for a vortex, which at zero time has a vorticity distribution of the form (2) with initial values of ζ_{0I} and w_0.

Of particular interest are the maximum values of v and the core radius a, where the maximum v occurs. From (7) these can be found to be

$$v = 0.384\, w_0\zeta_{0I}/(1+t')^{1/2} \tag{9}$$

$$a = 1.35\, w_0\,(1+t')^{1/2} \tag{10}$$

Note that $\Gamma(a)$ is given by $2\pi a v_{\max}$, or

$$\Gamma(a) = 3.25\, w_0^2\zeta_{0I}$$

From (8), the total vortex strength Γ_∞ is obtained as r approaches ∞:

$$\Gamma_\infty = \pi w_0^2\zeta_{0I}/\ln 2 \tag{11}$$

Hence,

$$\Gamma(a) = 0.716\,\Gamma_\infty \tag{12}$$

The preceding is a modification of Lamb's solution[7] in order to account for a known vorticity distribution at time $t = 0$. Rouse and Hsu[8] object to Lamb's solution since it requires an infinite amount of energy to establish it, i.e., the kinetic energy per unit length of vortex E is infinite. E is given by

$$E = \rho\int_0^\infty rv^2\,dr \tag{13}$$

However, Ref. 9 and others have shown E to be finite when one considers a finite wing with two oppositely rotating trailing vortices.

Rouse and Hsu derived a solution to (1) by allowing a cylinder to rotate for a finite time, thereby generating the rotational flow. The ensuing motion, following the stopping of the cylinder, then describes the decay of the vortex. This results, however, in a circulation function that reaches a maximum at some radius and then approaches zero asymptotically with increasing radius. From the standpoint of Helmholz's laws of vortex continuity, this circulation function raises some questions concerning the applicability of Rouse and Hsu's model to the present case since Γ_∞ should equal the midspan value of the wing's bound circulation.

From Eq. (9), one can write

$$1/v^2 = (1/v_0^2) + (4\nu_e\, t \ln 2/v_0^2 w_0^2) \tag{14}$$

In the preceding, ν has been replaced by an effective kinematic viscosity ν_e in view of the presumed turbulent nature of the flow.

If the time t is replaced by the distance downstream of the wing Z divided by the freestream velocity, Eq. (14) becomes

$$1/v^2 = (1/v_0^2) + (4\nu_e \ln 2/v_0^2 w_0^2 V)Z \tag{15}$$

Thus the preceding predicts that a plot of $1/v^2$ as a function of the distance downstream of the aircraft should result in a straight line, the slope of which is proportional to the effective kinematic viscosity. ν_e can also be determined from the variation of the core radius with distance. According to (10),

$$a^2 = a_0^2 + 5.05\,\nu_e(Z/V) \tag{16}$$

Hoffman and Joubert[12] present an alternate approach to the analysis of a vortex. This analysis suggests that, except for a small eye at the center of the vortex and for very large radii, the behavior of the rotational flow in the vortex core is independent of viscosity. This leads to a predicted logarithmic variation of Γ with r. Also their analysis suggests that turbulent vortices will exhibit geometric similarity.

According to Ref. 12, we can write Γ in the form

$$\Gamma/\Gamma(a) = \ln(r/a) + 1 \tag{17}$$

$\Gamma(a)$ is the value of the circulation at the radius for maximum v. Consider for the moment the derivative $d\Gamma/d(\ln r)$. Since $\Gamma = 2\pi rv$,

$$\frac{d\,\Gamma}{d(\ln r)} = r\frac{d\Gamma}{dr} = 2\pi rv + 2\pi r^2\frac{dv}{dr}$$

At the radius a, dv/dr is equal to zero and $2\pi av = \Gamma(a)$. Hence,

$$[d\Gamma/d\ln r]_a = \Gamma(a) \tag{18}$$

The preceding holds irrespective of the Γ distribution.

If a decaying vortex maintains geometric similarity we can write

$$\zeta/\zeta_0 = f\,(r/a) \tag{19}$$

Therefore, from (4) and (5),

$$\Gamma(r) = a^2\zeta_0 f(r/a) \tag{20}$$

$$v(r) = a\zeta_0 g(r/a) \tag{21}$$

$f(r/a)$ and $g(r/a)$ are unique functions of the dimensionless

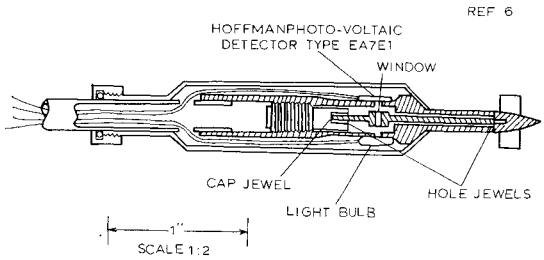

Fig. 1 Vortex meter.

radius r/a. If (20) is assumed to have a limit as $r \to \infty$, so that $\Gamma \to \Gamma_\infty$, then it follows that

$$\Gamma(a) = \text{const} \times \Gamma_\infty \tag{22}$$

Since Γ_∞ is a constant, this leads to $a^2\zeta_0$ and the product va being constant, if the assumption of geometrical similarity is true.

Description of Test Program

The test program was designed to provide data on the vortex sheet shed initially from the wing's trailing edge, on how this sheet rolls up to form the two trailing vortices, and on how these trailing vortices dissipate with distance downstream of the aircraft. Such data were obtained for wings of different aspect ratios and taper ratios operating over a range of lift coefficient and Reynolds numbers. Four pieces of special instrumentation worthy of description were developed for this study.

Vortex Meter

Described more completely in Ref. 1, this vorticity probe is shown in Fig. 1. It consists of four, unpitched vanes mounted on a hub attached to a shaft supported between two jeweled-bearings. A small light is shone through a window in the shaft onto a small photocell. In order to reduce windage losses, the window was filled with a polished clear plastic, and the clearance between the shaft and housing was made as large as was feasible. For wind-tunnel model tests, the diameter of the vanes was $\frac{3}{8}$ in. For flight tests, the diameter was increased to $\frac{3}{4}$ in. The rotational velocity of the vanes is measured by counting electronically the voltage pulses from the photocell. Ideally, the vanes rotate with an angular velocity equal to half of the fluid vorticity. In practice, the angular velocity is slightly different from this because of the finite size of the vanes and the friction in the system. The calibration of the meter is discussed in Ref. 2.

The vortex meter performed well throughout both the model and in-flight tests. The calibration was checked periodically by installing a set of pitched vanes ahead of it to impart a known rotation to the flow. Dryness of the bearings produced a noticeable change in its performance. By carefully adjusting the pressure on the aft bearing and by periodic lubrication, its calibration could be easily maintained. Rotational speeds as high as 32,000 rpm were measured with this probe.

Velocity Meter

The velocity meter is described in detail in Ref. 3. It consists of a small, 5-holed, pitot-static tube supported on two, orthogonal circular-arc tracks having their centers-of-curvature at the total-head inlet. The arcs are driven by small d.c. motors with their positions measured by a servotransmitter-counter combination. For wind-tunnel tests, the velocity meter, like the vortex meter, was supported on an x-y traversing mechanism so that it could be precisely positioned in a plane downstream of the wing. At each point in the flow, the angular position of the probe was adjusted so that the pitot tube was aligned with the resultant velocity. In this way, all velocity components associated with the vortex could be determined.

Tuft Grid

In order to observe the vortex far downstream of an aircraft, a large tuft grid was constructed. This 10- × 10-ft grid with 2-in.-long wool tufts spaced 1 in. apart was mounted on a trailer so that it could be easily positioned alongside of the runway with the plane of the grid perpendicular to the runway. The center of the grid was 15 ft above the ground. By flying the test aircraft to one side and slightly above the grid, the trailing vortices would move downward and laterally outward intersecting the grid. By flying progressively further and further away from the grid, the trailing vortices could be observed. The grid proved an effective means of visually observing the vortices, and a movie was made of its action which is available from the author on loan. A still photo of the grid, showing a vortex, is presented in Fig. 2.

Vortimeter

For measuring the velocity distribution far downstream of the test aircraft, an instrument labeled the vortimeter was designed and constructed. This instrument, described in more detail in Ref. 4, is pictured alongside of the tuft grid in Fig. 3. It consists of a vertical array of 30, 1-ft-long, $\frac{1}{4}$-in.-diam cylinders. Each cylinder is supported on strain-gaged flexures so that the aerodynamic drag on each cylinder can be measured. Hence the velocity distribution through the vortex can be determined as the vortex moves through the array by measuring the output from each cylinder on an oscillograph. The apparatus is designed so that the vertical spacing between cylinders can be varied.

Testing Procedure

Model testing was performed principally in the Pennsylvania State University's 3- × 3-ft subsonic wind tunnel at a speed of 75 mph. For these tests, semiwing models were

Fig. 2 Vortex shown by tuft grid.

Table 1 Test aircraft specifications

	0-1	Cherokee
Test weight, lb	2200	1900
Wing area, ft^2	174	160
Aspect ratio	7.45	5.62
Midspan chord, ft	5.33	5.25
$dC_L/d\alpha$	4.77	4.18
C_{l_0}/C_L	1.17	1.19

mounted vertically from the floor. Surveys in transverse planes at varying distances downstream of the test wing were made using either the vortex meter or the velocity meter. Considerably more data were obtained with the former, since the use of the velocity meter was tedious and time consuming. The velocity meter was used primarily in the study of vortex breakdown reported in Ref. 3.

Flight testing was performed using a U.S. Army 0-1 aircraft and a Piper Cherokee. Measurement of the trailing vortices several thousands of feet downstream of each aircraft was made using the vortimeter and the tuft grid. In addition, the vortex meter was supported on the 0-1 and vorticity surveys made in proximity of the trailing edge of its wing. A photograph of this installation is shown in Fig. 4. The vortex meter could be moved vertically in flight. For lateral or longitudinal movement, ground adjustment was necessary. Model testing included models of the 0-1 and Cherokee wings as well as wings of varying aspect ratios and taper ratios.[5]

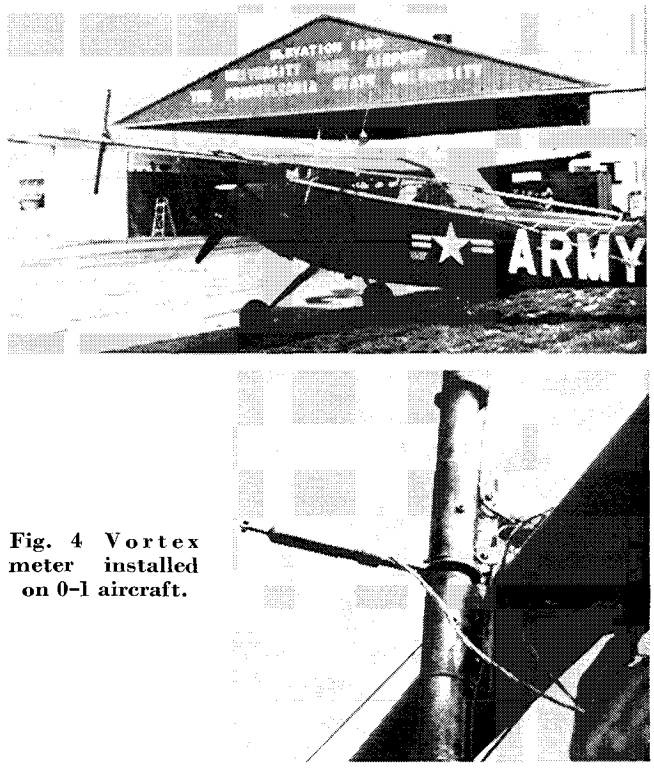

Fig. 4 Vortex meter installed on 0-1 aircraft.

Experimental Results

Initial formation of vortex systems: Typical measurements obtained with the vortex meter are presented in Fig. 5 for the $\frac{1}{12}$ scale model of the 0–1 wing. Comparable measurements at the same lift coefficient for the full-scale aircraft are shown in Fig. 6. These data are taken from Ref. 6. The geometry of the 0-1 and the Cherokee are given in Table 1. It is interesting to note that at a distance of only 20% of the midchord behind the trailing edge a well-defined tip vortex already exists. From these figures, the roll-up of the vortex sheet with distance aft into a progressively stronger tip vortex can be clearly seen. At less than a chord length downstream, 90% of the measurable circulation of the vortex system is contained in the tip vortices.

The magnitude of the vorticity in the vortex system for a full-scale aircraft is seen to be approximately a third of that for the model. Also, at corresponding downstream distances, the vortex sheet behind the full-scale aircraft appears to be more completely rolled up. However this may be the result of the vorticity in the vortex sheet for the full-scale aircraft falling below the threshold of the vortex-meter sensitivity.

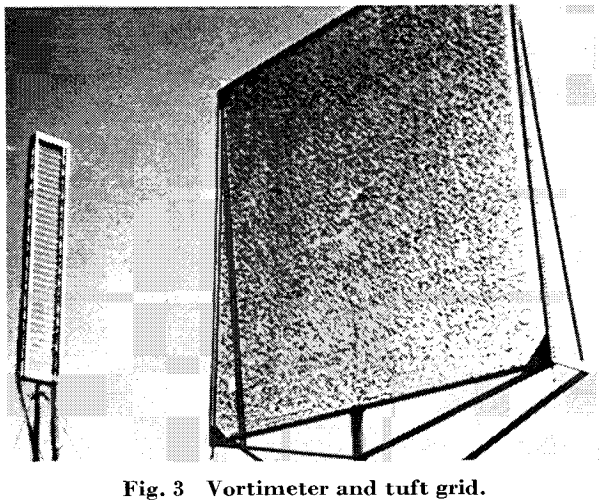

Fig. 3 Vortimeter and tuft grid.

The vorticity contours for the full-scale aircraft are somewhat less certain than for the model because of difficulties in maintaining the heading of the aircraft. From Fig. 6, the extent of the rotational flow in the tip vortex is seen to be only about 6 in. Therefore, at a distance of 6 ft behind the trailing edge, a heading change of only 3° can move the probe entirely through the vortex. Needless to say, all flight testing was performed in stable air.

Tangler's measurement of v_0/V are presented in Fig. 7 for Z/c_0 values of 0.6 to 1.1. In addition to the full-scale values,

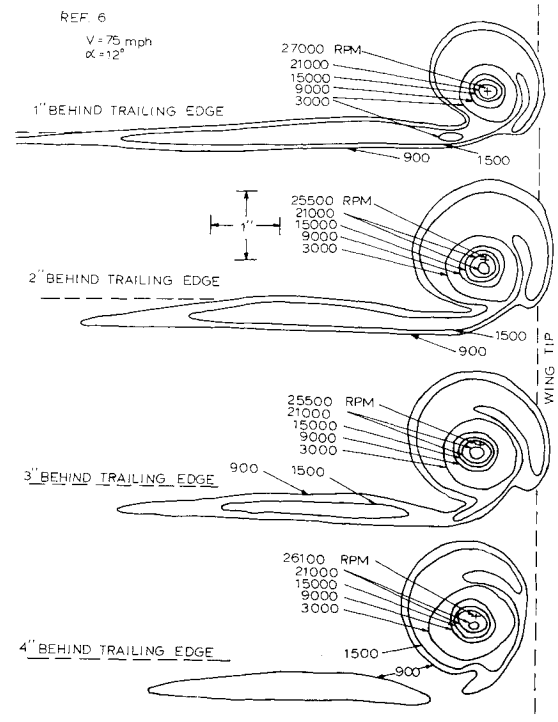

Fig. 5 Vorticity contours for the $\frac{1}{12}$ scale 0-1 aircraft wing.

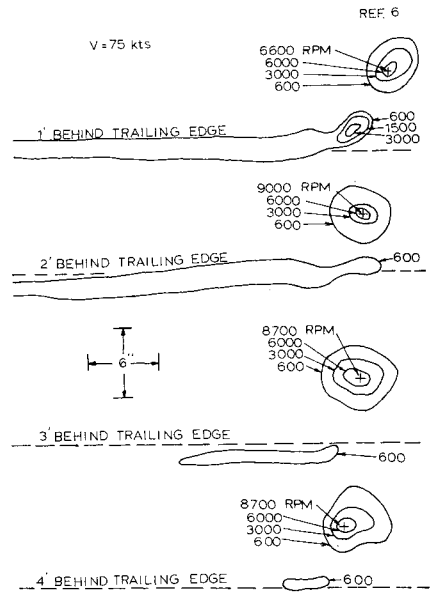

Fig. 6 Vorticity contours for the full-scale 0-1 aircraft.

model results of Ref. 4 obtained with the vortimeter also are included. As can be seen, Tangler's and Sherrieb's data are consistent and only about 10% lower than Grow's. Incidentally, an error in C_L present in Ref. 6 has been corrected in this figure.

Considerable model testing was performed in Ref. 5 for wings with aspect ratios varying from 2.0 to 6.0 and taper ratios from 0 to 1.0. Measurements were made of the vortex geometry at approximately 4 chord-lengths downstream of the trailing edge. At this location the vortex sheet is completely rolled up into discrete vortices. A typical variation of the axisymmetric vorticity as measured along a radius passing through the center of the vortex is shown in Fig. 8.

In view of Eq. (2), all of the vorticity data taken in proximity to the wing could be fitted by, and were analyzed on the basis of, an exponential fit of the form

$$\zeta = \zeta_0 \exp[-(r/w)^n \ln 2] \tag{23}$$

A fit, and subsequent numerical integration, of the vorticity data was made using a high-speed digital computer to give $v(r)$.

For $r = \infty$, Eq. (23) can be integrated immediately to give the total vortex strength:

$$\Gamma_\infty = [2\pi\zeta_0 w^2/n(\ln 2)^{2/n}]\gamma(2/n) \tag{24}$$

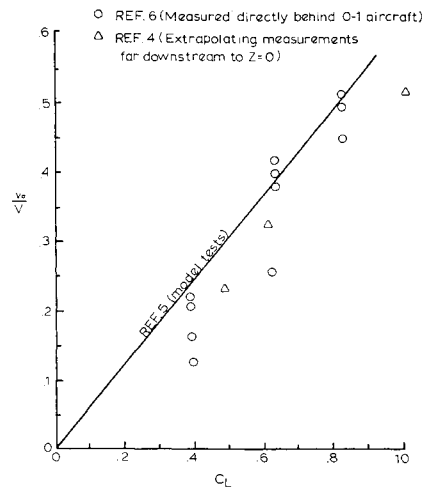

Fig. 7 Initial tangential velocity ratio as a function of lift coefficient.

where $\gamma(2/n)$ = gamma function of argument $(2/n)$. For the particular case where $n = 2$, Eqs. (6–12) apply with $t' = 0$.

The test wings were untwisted with NACA 0012 airfoil sections. The tips were formed by revolving the airfoil section around the chord line. Taper ratios from 0 to 1 for a fixed aspect ratio of 6 were investigated, as well as aspect ratios from 2 to 6 for a fixed taper ratio of 1. All of the model data were taken at a Reynolds number based on the midchord of approximately 3.5×10^5.

When reduced on the basis of the wing C_L and the average chord $\bar{c}$, the data of Ref. 5 exhibit some interesting trends. First is the fact that v_0/V, for aspect ratios greater than 4, is independent of aspect ratio and taper ratio and is given by

$$v_0/V = 0.625C_L \qquad (R_e = 3.5 \times 10^5) \tag{25}$$

Below an aspect ratio of 4, v_0/V tends to increase reaching a value of $0.7C_H$ at an aspect ratio of 2.

The ratio of the half-radius w to the mean chord $\bar{c}$ for all aspect ratio-taper ratio combinations studied in Ref. 5 is fitted by

$$w_0/\bar{c} = 0.02 + 0.035C_L \qquad (R_e = 3.5 \times 10^5) \tag{26}$$

The measured values of the exponent n did not exhibit any trend with C_L, aspect ratio, or taper ratio. From a sample of 250 points, n had an average value of 2.19.

Decay of Vortex

Knowing the initial geometry and strength of the trailing vortex, one is next faced with the question of its dissipation or its persistence. To answer this question in detail, data reported in Ref. 4 were obtained using the vortimeter. Velocity distributions through the trailing vortices shed by the 0-1 and Cherokee aircraft were measured several thousand feet downstream of the aircraft. Typical experimental measurements of the tangential velocity through the vortex at several distances downstream of the 0-1 are shown in Fig. 9.

From such data, Figs. 10 and 11 were obtained on the variation of core diameter and maximum tangential velocity. Although there is some scatter in the data of Figs. 9–11, these data are probably the most significant obtained to date concerning vortex decay. Previous investigators[10,11] have attempted similar measurements by flying one aircraft instrumented with a probe through the wake of another. However, the size of the vortex and the fact that it moves with the random wind make it difficult with this experimental approach to define the vortex with any precision. Figure 12 is also taken from Ref. 4 and presents the radial distribution of circulation through the trailing vortex as determined from the measured velocity distribution.

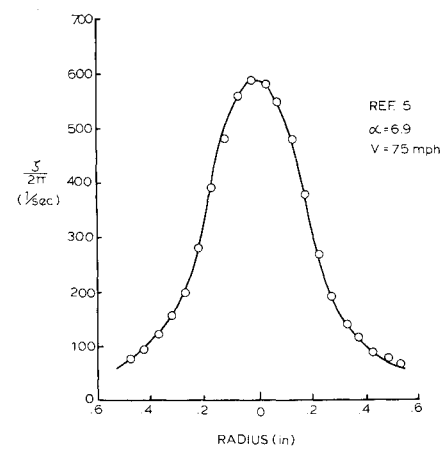

Fig. 8 Typical vorticity distribution through a vortex.

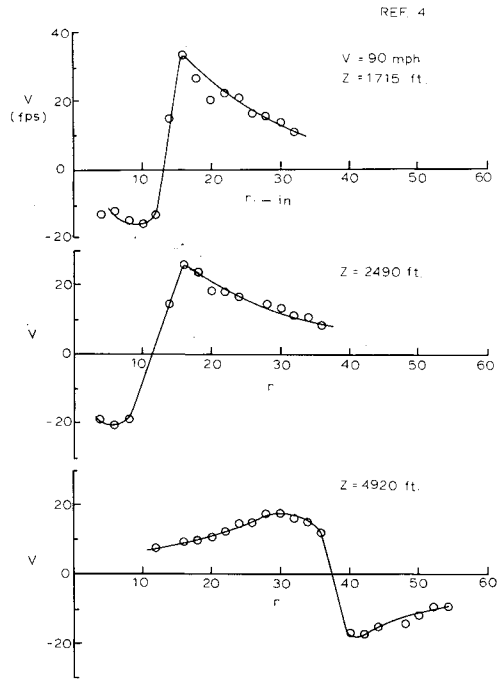

Fig. 9 Tangential velocity profiles through the vortex of the 0-1 aircraft at several downstream distances.

Analysis of Data

The data of Figs. 10 and 11 were first plotted on the basis of Eqs. (15) and (16). Even though there is more scatter in the data than one would like, the values of ν_e obtained from the $1/v^2$ plot not only appear to vary with V (approximately proportional to V^2) but are completely incompatible with the values obtained from the $1/a^2$ plot.

Next, the data of Fig. 12 were replotted against $\ln r$ as shown in Fig. 13. Observe that Γ vs $\ln r$ for the three velocities is linear as predicted by Hoffman and Joubert. Also note that the values of $\Gamma(a)$ obtained from the slope of the curves are nearly a constant fraction of Γ_∞. Next, consider Fig. 14 obtained from Figs. 10 and 11. Although there is some scatter in the results, it appears that $\Gamma(a)$ is not a function of Z but is constant with a value of approximately 0.16 Γ_∞, which checks the results from Fig. 13.

Now consider Fig. 15, which is typical of the model test results. This figure, replotted from Fig. 20 of Ref. 2, again exhibits a constant slope over a large radial extent. However, for this case $\Gamma(a)/\Gamma_\infty$ is approximately 0.77, which is considerably higher than the fraction obtained from Sherrieb's data and more nearly equal to the value of 0.716 predicted by Eq. (12).

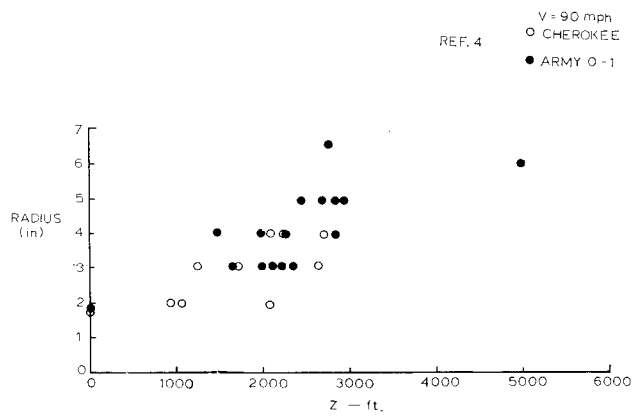

Fig. 10 Variation of core radius with downstream distance.

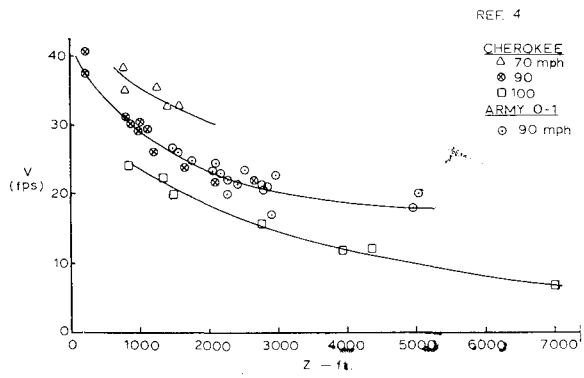

Fig. 11 Variation of maximum tangential velocity with downstream distance.

After considering these results and the comments of Ref. 12, it appears that the vortex that is initially generated behind the wing can be described by Eqs. (6–12). However, at some downstream distance, depending on the Reynolds number, it undergoes a transition to the form of Eq. (17). Although one might liken this to a transition from a laminar to a turbulent boundary layer, it is difficult to believe that the flow in the vortex is initially laminar. Certainly, for the case of Fig. 15, the boundary layer shed from the trailing edge is turbulent, and it is this boundary layer that forms the vortex sheet that ultimately rolls up into the core. Possibly, the change from an exponential circulation to a logarithmic one is associated with vortex breakdown. The results of Ref. 3 and others indicate a drastic modification to the centerline vorticity over a relatively short downstream distance. Such a behavior is shown in Fig. 16, taken from Ref. 3. These are model results obtained with the vortex meter. Notice that, after breakdown, negative rotations actually were measured in the center of the vortex. This is certainly in the direction of the logarithmic distribution, which predicts much lower ζ values near the center than does the exponential distribution. However, the $\Gamma(a)$ values before and after breakdown from Fig. 13 are not significantly different; at least, not by comparison with Figs. 11 and 12.

Hoffman and Joubert's hypotheses are apparently confirmed by the logarithmic Γ distribution. Hence one might hope that geometric similarity holds for the entire vortex system. Figures 7 and 11 were replotted in the form of Fig. 17, and indeed the three separate curves of Fig. 11 collapse to a single curve. Figures 7 and 17 are very significant, as they, together with the fact that $\Gamma(a) = 0.16\ \Gamma_\infty$, form the basis for predicting the vortex geometry downstream of an aircraft.

Whether or not c is really the proper reference length to use is open to question. A word of caution in this regard must be added as a result of preliminary findings from Ref. 13. Here, porous wing tips were added to the 0-1 aircraft in an attempt to increase the size of the core radius. Indeed, a sig-

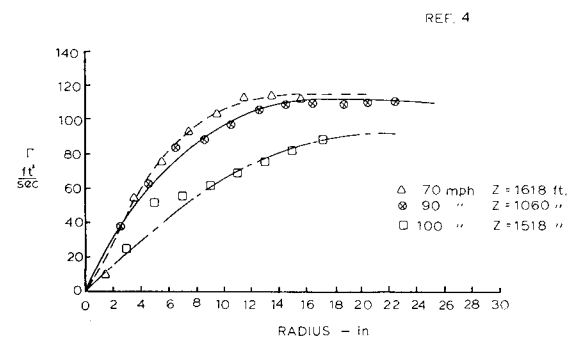

Fig. 12 Radial distribution of circulation through the vortex at several downstream distances.

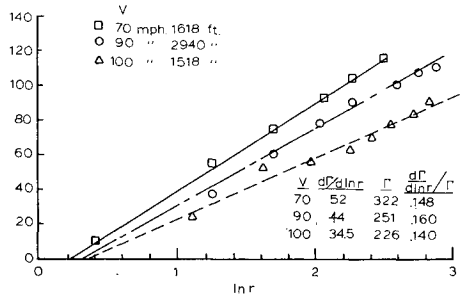

Fig. 13 Circulation vs lnr for full-scale.

nificant increase in a_0 and decrease in v_0 were accomplished. However, far downstream, v was reduced only slightly. Hence, these results, plotted in the form of Fig. 17, fall above the curve shown there. This suggests that possibly an initial characteristic dimension of the vortex such as a_0 would be a better choice as a reference length. Neither this question nor the effect of Reynolds number on Figs. 7 and 17 and on $\Gamma(a)/\Gamma_\infty$ can be resolved by the present data. Here is an area worthy of further investigation.

It would appear, in final retrospect, that the model data obtained during the course of this study are of limited value, since the distribution of the vortex changes from an exponential form at the model Reynolds number to the logarithmic form for the full-scale Reynolds number. However, the data do suggest that aspect-ratio and taper-ratio effects on v/V are not severe.

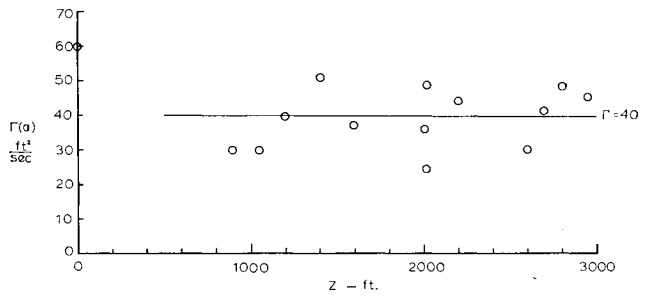

Fig. 14 Measured core circulation as a function of downstream distance.

It should be pointed out that a certain inconsistency exists in the data. Equations (25) and (26), as well as Ref. 6, indicate that both v_0 and a_0 increase linearly with C_L. Obviously if $\Gamma(a)$ is to remain a constant fraction of Γ_∞, then the product of a and v must be directly proportional to C_L. In answer to this possible criticism it can only be suggested that, regardless of the details of the vortex formation, the vorticity tends to the logarithmic distribution such that $\Gamma(a)$ increases linearly with C_L.

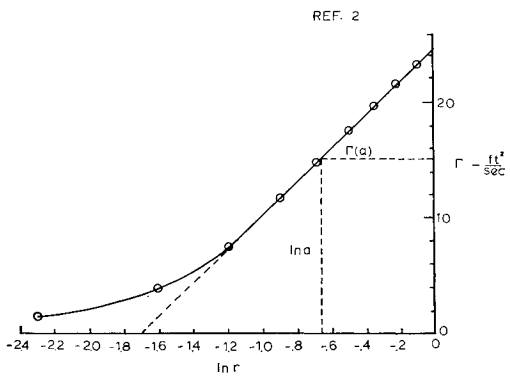

Fig. 15 Circulation vs lnr for model scale.

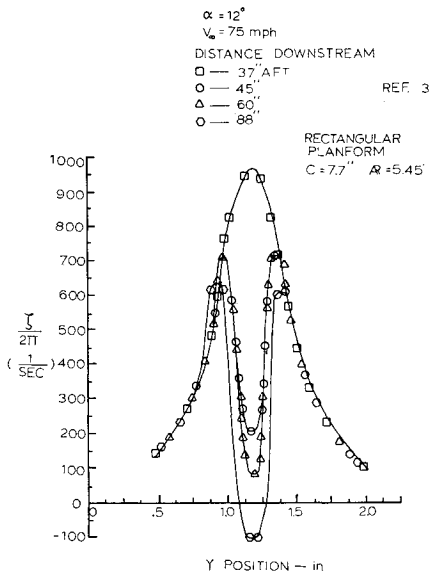

Fig. 16 Effect of vortex breakdown on vorticity.

Illustrative Calculation

For illustrative purposes, consider a typical "jumbo-jet" having a wing loading of 120 psf, a wing area of 6000 ft² and a span of 220 ft. The average chord would be 27 ft. For a taper ratio of $\frac{1}{2}$, the midchord would be 36.4 ft. For an operating lift coefficient of 2.0, v_0/V from Fig. 7 will be 1.05. At standard sea-level conditions, the aircraft velocity will be 225 fps or 153 mph, so that v_0 will be 236 fps. Γ_∞ is $c_0 c_{l_0} V/2$. Assuming $C_{l_0}/C_L = 1.1$, $\Gamma = 9000$ ft²/sec. Hence $\Gamma(a) = 0.16\ \Gamma_\infty = 1440$ ft²/sec. The initial core radius will be $a_0 = \Gamma(a)/2\pi v_0 = 0.97$ ft.

Now consider what the vortex structure will look like 1 min after the passage of the aircraft. This corresponds to a downstream distance of 13,500 ft, or $Z/\bar{c} = 500$. From Fig. 17, $v/v_0 = 0.48$ so that $v = 113$ fps. The core radius varies inversely with v. Hence $a = a_0/0.48 = 2.02$ ft.

Γ is then calculated from Eq. (17) as

$$\Gamma/1440 = \ln(r/2.02) + 1$$

The velocity distribution is next calculated from $v = \Gamma/2\pi r$.

The predictions of Fig. 18 were made for 1, 3, and 5 min., in the manner described earlier in this section. As can be seen, even 5 min after passage, the velocity field is quite severe. Were a typical light aircraft to penetrate this field such that its axis were aligned with that of the vortex, the upsetting rolling moment would be approximately twice the maximum rolling moment available from the aileron control. For comparison purposes, an estimate is also included on Fig. 18 for a typical current jet transport.

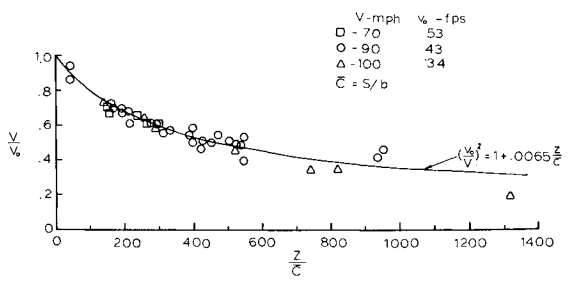

Fig. 17 Decay of maximum velocity with downstream distance.

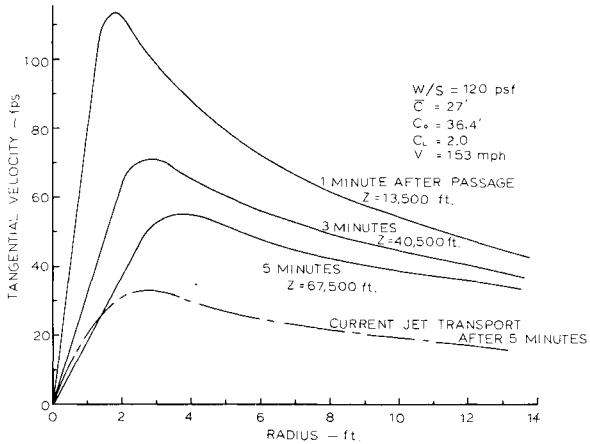

Fig. 18 Prediction of velocity distribution through the trailing vortex of large aircraft.

Conclusions

From the results of this study, it is concluded that the maximum tangential velocity in the core of the vortex trailing from an aircraft decreases with distance downstream of the aircraft in accordance with Fig. 17. At large distances, this decrease is approximately in inverse proportion to the square root of the distance. The core size of the vortex increases with distance so as to keep the product of the core radius and maximum tangential velocity a constant. v and a, expressed as a fraction of their initial values close behind the aircraft, are found to be functions only of the downstream distance independent of the aircraft velocity.

The circulation at the core was found to remain constant with downstream distance and equal to 16% of the theoretical total strength of the vortex. Also the circulation distribution through the vortex core was found to be logarithmic with the radius. It is concluded, therefore, that the vortex decay is not dependent on viscosity but indeed exhibits the geometric similarity just described. This statement holds for large Reynold's numbers based on the aircraft wing chord of at least 3×10^6 but may not hold for smaller Reynolds numbers. Model tests at a R_e of approximately 3×10^5 show the circulation distribution to vary exponentially with radius in agreement with predictions based on the Navier-Stokes equations.

References

[1] May, D. M., "The Development of a Vortex Meter," M.S. thesis, 1964, Pennsylvania State Univ., University Park, Pa.

[2] Spencer, R. H., Sternfeld, H., and McCormick, B. W., "Tip Vortex Core Thickening for Application to Helicopter Rotor Noise Reduction," TR 66–1, Sept. 1966, USAAVLABS.

[3] Logan, A. H., "A Solution to the Vortex Breakdown Phenomenon in a Trailing Line Vortex," M.S. thesis, 1966, Pennsylvania State Univ., University Park, Pa.

[4] Sherrieb, H. E., "Decay of Trailing Vortices," M.S. thesis, 1967, Pennsylvania State Univ., University Park, Pa.

[5] Grow, T. L., "The Effect of Wing Geometry and Lower Surface Boundary Layer on the Rolled-Up Vortex," M.S. thesis, 1967, Pennsylvania State Univ., University Park, Pa.

[6] Tangler, J. L., "A Study of the Vortex Sheet Immediately behind an Aircraft Wing," M.S. thesis, 1965, Pennsylvania State Univ., University Park, Pa.

[7] Lamb, H., *Hydrodynamics*, 6th ed., Dover, New York, 1945, pp. 591–592.

[8] Rouse, H. and Hsu, H., "On the Growth and Decay of a Vortex Filament," *Proceedings of the 1st U.S. National Congress of Applied Mechanics*, American Society of Mechanical Engineers, 1950.

[9] McCormick, B. W., "A Study of the Minimum Pressure in a Trailing Vortex System," Ph.D. dissertation, 1954, Pennsylvania State Univ., University Park, Pa.

[10] Rose, R. and Dee, F. W., "Aircraft Vortex Wakes and Their Effects on Aircraft," CP 795, 1965, Aeronautical Research Council.

[11] Wetmore, J. W. and Reeder, J. P., "Aircraft Vortex Wakes in Relating to Terminal Operations," TN D-1777, April 1963, NASA.

[12] Hoffman, E. R. and Joubert, P. N., "Turbulent Line Vortices," *Journal of Fluid Mechanics*, Vol. 16, Pt. 3, July 1963, pp. 395–411.

[13] Smith, H. C., "Effects of a Porous Wingtip on an Aircraft Trailing Vortex," M.S. thesis, 1967, Pennsylvania State Univ., University Park, Pa.